ISSN 0915-633X

NATIONAL INSTITUTE FOR FUSION SCIENCE

Molecular Dynamics Simulation of Structure Formation of Short Chain Molecules

S. Fujiwara and T. Sato

(Received - Oct. 28, 1998)

NIFS-577 Nov. 1998

RESEARCH REPORT
NIFS Series

NAGOYA, JAPAN

Molecular dynamics simulation of structure formation of short chain molecules

Susumu Fujiwara and Tetsuya Sato

Theory and Computer Simulation Center, National Institute for Fusion Science, 322-6 Oroshi-cho, Toki-shi 509-5292, Japan

Abstract

Molecular dynamics simulations are carried out to study the structure formation of 100 short chain molecules, each of which consists of 20 CH_2 groups. Our simulations show that the orientationally ordered structure is formed from a random configuration by quenching. The global orientational order starts to increase suddenly after a certain duration and grow in a stepwise fashion afterwards. This behavior is also found in the growth process of the local orientationally-ordered regions. It is found from the microscopic analysis of the structure formation process that parallel ordering of chain molecules starts to occur after the rigidity of chain molecules grows to some extent. From the analysis of the obtained orientationally ordered structure and the molecular mobility, we also find the following characteristic features: (i) The chain molecules are packed hexagonally at 400 K and the transition from the hexagonal phase toward the orthorhombic phase takes place as the temperature decreases. (ii) The *gauche* bonds in the same chain molecule tend to form *gauche* pairs. The *gauche* pairs with the same sign form the double *gauche* defects and those with the opposite sign form the kink defects. (iii) In the hexagonal phase, the chain molecules become longitudinally mobile. This result, which is obtained by the microscopic analysis of the chain motion, is the microscopic evidence to confirm the existence of the chain sliding diffusion in the hexagonal phase which underlies the sliding diffusion theory of polymer crystallization proposed by Hikosaka [M. Hikosaka, Polymer **28**, 1257 (1987); **31**, 458 (1990)].

Keywords: molecular dynamics simulation, chain molecule, structure formation, orientational order, conformational defects, molecular mobility

1 Introduction

Structure formation of chain molecules, such as *n*-alkanes and polyethylene chains, is a very interesting research topic in physics, chemistry, and biology and has attracted the attention of many researchers. Since chain molecules have many internal degrees of freedom, structure formation proceeds in a complex fashion. Intensive experimental studies have been made on various structure formation processes of chain molecules, such as crystallization of polymers [1–11] and surface freezing of oligomers [12–16]. The primary nucleation in the early stages of crystallization of polyethylene [3–5] and poly(ethylene terephthalate) [6–11] has been investigated by various time-resolved measurements. Wu *et al.* discovered the surface freezing phenomenon in *n*-alkanes [12–15] and *n*-alcohols [16] by x-ray scattering and surface tension measurements. Surface freezing is an interesting phenomenon that an ordered monolayer is formed on the free surface of a liquid above its bulk freezing point.

Although considerable experimental investigations have thus been made, it seems difficult to observe the detailed mechanisms of the structure formation of polymer chains *at the molecular level* by the present experimental techniques only. Computer simulation is one of the strongest tools for investigating the molecular process of the structure formation. Over the last decade, several computer simulation studies have been done on primary nucleation of a single polymer chain [17–19], structure formation of short chain molecules [20–23], surface ordering in liquid *n*-alkanes [24], and secondary nucleation on a growth surface of a polymer crystal [25, 26].

It is well known that surface structures of chain molecules play crucial roles in determining physical properties, such as adhesion and wetting. It is on the surface of the material that the structure formation such as crystal growth occurs. Therefore molecular simulation studies of chain-molecule systems with free surfaces are very important from the viewpoints both of chemical physics and of engineering. Although several simulation studies of systems with free surfaces have been made on the structure formation, little is known about the detailed molecular motion during the structure formation.

In our previous papers, we have performed the molecular dynamics (MD) simulations of short chain-molecule systems with free surfaces [21, 22]. It was found from our simulations that the orientationally ordered structure is formed at low temperature by a sudden cooling from a random configuration at high temperature and that the formation of the orientational order proceeds in a stepwise fashion. The purpose of this paper is to clarify the dynamical processes of the structure formation of short chain molecules *microscopically* and analyze the molecular mobility and the conformational defects in the obtained orientationally-ordered structure. With a view to investigating the structure formation processes microscopically, we carry out the MD simulation of 100 short chain molecules and analyze the growth process of the orientational order. This paper is organized as follows. In Sec. 2 we give a detailed description of our simulation model and method. Our simulation results are presented in Sec. 3. Summary and discussion are given in Sec. 4.

2 Model and Method

The present computational model is the same as that used in the previous works on the structure formation of short chain molecules [21, 22]. The model chain molecule consists of a sequence of CH_2 groups, which are treated as united atoms. The mass of each CH_2 group is 14 g/mol. The united atoms interact via the bonded potentials (bond-stretching, bond-bending and torsional potentials) and the van der Waals nonbonded potential (12-6 Lennard-Jones potential). The atomic force field used here is the DREIDING potential [27]: (i) the bond-stretching potential,

$$V_{\rm stretch}(d) = \frac{1}{2}k_{\rm d}(d-d_0)^2, \qquad (1)$$

where d_0 is the equilibrium bond length and d is the actual bond length, (ii) the bond-bending potential,

$$V_{\rm bend}(\theta) = \frac{1}{2}k_\theta(\theta-\theta_0)^2, \qquad (2)$$

where θ_0 is the equilibrium bond angle and θ is the bond angle between three adjacent atoms, (iii) the torsional potential,

$$V_{\rm torsion}(\phi) = \frac{1}{2}k_\phi\left[1-\cos(3\phi)\right], \qquad (3)$$

where ϕ is the dihedral angle formed by four consecutive atoms, and (iv) the 12-6 Lennard-Jones potential between atoms separated by more than two bonds along the same chain and between atoms in different chains,

$$V_{\rm LJ}(r) = 4\epsilon\left[\left(\frac{\sigma}{r}\right)^{12}-\left(\frac{\sigma}{r}\right)^{6}\right], \qquad (4)$$

where r is the distance between atoms. The values of all the potential parameters are listed in Table 1. The equations of motion are solved numerically using the velocity version of the Verlet algorithm [28] and apply the Nosé-Hoover method in order to keep the temperature of the system constant [29–31]. The integration time step and the relaxation constant for the heat bath variable are 1.0 fs and 0.1 ps, respectively. The cutoff distance for the 12-6 Lennard-Jones potential is 10.5 Å. A hundred chain molecules, each of which consists of 20 CH_2 groups, are placed in a vacuum and other molecules such as solvent molecules are not considered. The total momentum and the total angular momentum are taken to be zero in order to cancel overall translation and rotation of chain molecules. The MD simulations are carried out by the following procedure. At first, we provide a random configuration of 100 short chain molecules at high temperature ($T = 700$ K). The system is then quenched to $T = 400$ K and subsequently it is cooled stepwise to $T = 100$ K by 100 degrees. A simulation of 2 ns (2×10^6 time steps) is performed at each temperature.

In the following section, we describe our simulation results in detail. To begin with, we investigate the formation process of the global orientational order (Sec. 3.1). Then the microscopic analysis of the structure formation processes is made (Sec. 3.2). Finally we study the molecular mobility and the conformational defects in the obtained orientationally-ordered structure (Sec. 3.3).

3 Results

3.1 Formation process of global orientational order

3.1.1 Chain configuration

Snapshots of the chain configuration are shown in Fig. 1 at various times ($t = 1$, 200 and 2000 ps) for $T = 400$ K. The a, b and c axes respectively correspond to the crystallographic a, b and c axes in the orthorhombic system and are determined by the inner 37 chains (Fig. 2) after the orientationally-ordered structure is formed [21]. Figure 1 indicates the following features: (i) In the early time ($t = 1$ ps), the chain molecules take a *random* configuration. (ii) As time elapses, growth of the local orientationally-ordered clusters is observed in several positions ($t = 200$ ps). (iii) At last, several clusters coalesce into a large cluster and a highly ordered structure is formed ($t = 2000$ ps). In the ordered structure, almost all the bonds are in the *trans* state.

We show, in Fig. 2, the center-of-mass positions of individual chain molecules averaged between 1500 ps and 2000 ps for $T = 400$ K. The calculated lattice constants a and b are respectively $a = 0.750$ nm and $b = 0.433$ nm. Therefore the ratio a/b is calculated as $a/b = 1.733 \approx \sqrt{3}$, which indicates that chain molecules are packed hexagonally at $T = 400$ K.

3.1.2 Global orientational order parameter

In order to investigate the growth process of the global orientational order, we calculate the global orientational order parameter P_2, which is defined by

$$P_2 = \left\langle \frac{3\cos^2\psi - 1}{2} \right\rangle_{\text{bond}}, \tag{5}$$

where ψ is the angle between two adjacent sub-bond vectors and $\langle \cdots \rangle_{\text{bond}}$ denotes the average over all pairs of sub-bonds. The sub-bond vector is the vector formed by connecting centers of two adjacent bonds along the same chain. The parameter P_2 takes a value of 1.0 when all sub-bonds are parallel and that of 0.0 when sub-bonds are randomly oriented. We show the time dependence of the global orientational order parameter P_2 in Fig. 3. Up to $t \approx 150$ ps, the parameter P_2 takes a value near zero, which means that there is no global orientational order in this time region. After $t = 150$ ps, P_2 increases sharply, which indicates that the global orientational order starts to grow suddenly after a certain duration. This fact is also found in the MD simulation of a bulk short chain-molecule system [23].

3.2 Microscopic analysis of the structure formation process

3.2.1 Conformational change

In order to investigate the structure formation process at the molecular level, we first examine how the conformational change takes place. In Fig. 4, we show the time dependence of the fraction of the *trans* states ($|\phi| < \pi/3$), P_{trans}, at $T = 400$ K. This figure tells us that P_{trans} increases logarithmically up to $t \approx 350$ ps and is almost constant afterwards. It is found that the fraction of the *trans* states increases even in the duration when the global orientational order does not exist (see Fig. 3).

We then calculate the distribution of the size of the *trans* segments, i.e., the number of consecutive *trans* bonds, n_{tr}, in order to investigate the growth process of the *rigidity* of chain molecules. The distribution of the size of the *trans* segments $P(n_{\text{tr}})$ is normalized as

$$\sum_{n_{\text{tr}}=1}^{n-3} P(n_{\text{tr}}) = 1, \tag{6}$$

where n is the number of united atoms per chain molecule ($n = 20$ in this work). The distribution $P(n_{\text{tr}})$ is shown in Fig. 5 at various times for $T = 400$ K. At $t = 0$ ps, $P(n_{\text{tr}})$ decreases with the increase of the size n_{tr} and almost all the *trans* segments are small: $P(n_{\text{tr}} > 10) \approx 0$. With the elapse of time, the fraction of the *trans* segments with large n_{tr} increases while that with small n_{tr} decreases ($t = 10$, 20 and 100 ps). At $t = 200$ ps, the fraction of the *trans* segments with $n_{\text{tr}} \leq 16$ becomes small and $P(n_{\text{tr}} = 17)$, which means *all-trans* conformation, reaches about 0.4. At $t = 2000$ ps, the distribution $P(n_{\text{tr}} = 17)$ exceeds 0.7, which indicates that most chain molecules are in the *all-trans* conformation. We show, in Fig. 6, the average size of the *trans* segments, $\overline{n_{\text{tr}}}$, which is defined by

$$\overline{n_{\text{tr}}} = \sum_{n_{\text{tr}}=1}^{n-3} n_{\text{tr}} P(n_{\text{tr}}) \tag{7}$$

and satisfies $1 \leq \overline{n_{\text{tr}}} \leq n - 3 (= 17)$, as a function of time at $T = 400$ K. The average size $\overline{n_{\text{tr}}}$ starts to increase sharply at $t \approx 70$ ps and becomes almost constant after $t \approx 350$ ps. By making a comparison between the time evolution of P_{trans} (Fig. 4) and that of $\overline{n_{\text{tr}}}$ (Fig. 6), it is clearly found that at first the transition from the *gauche* state to the *trans* state takes place and after that the rigidity of chain molecules starts to grow. Judging from the fact that the rigidity of chain molecules increases in the duration when no global orientational order exists, it is concluded that growth of the *intrachain* orientational order, i.e., the rigidity of chain molecules, starts to proceed prior to that of the *interchain* orientational order, i.e., parallel ordering. This is ascertained again in the later subsection (Sec. 3.2.3). Therefore we may say that parallel alignment of chain molecules is triggered off by the increase of their rigidity. This finding is also observed in experiments of *long* chain molecules such as polyethylene [3–5] and poly(ethylene terephthalate) [6–9].

3.2.2 Spatial distribution of *gauche* bonds

In this subsection, we study the spatial distribution of *gauche* bonds ($|\phi| > \pi/3$). Before discussing the spatial distribution of *gauche* bonds, we calculate the number of isolated *gauche* bonds. The isolated *gauche* bond can be defined as the only *gauche* bond that a chain molecule possesses. The average number of *gauche* bonds n_{G}, isolated *gauche* bonds n_{IG} and their ratio $n_{\text{IG}}/n_{\text{G}}$ for several time intervals are shown in Table 2 at $T = 400$ K. In the initial time region ($t = 0 \sim 500$ ps), about one third of the *gauche* bonds are the isolated ones. As time elapses, the ratio $n_{\text{IG}}/n_{\text{G}}$ increases whereas the total number of *gauche* bonds n_{G} reduces. In the time region of $t = 1500 \sim 2000$ ps, the ratio of the isolated *gauche* bonds to the total *gauche* bonds reaches two thirds, which indicates that most of the *gauche* bonds are isolated.

In order to investigate the intrachain spatial correlation of *gauche* bonds, we calculate the pair distribution function of *gauche* bonds $p(m)$, where m is the bond separation, that is, $m - 1$ represents the number of bonds present between the *gauche* pairs. The pair distribution function $p(m)$ is normalized as

$$\sum_{m=1}^{n-4} p(m) = 1. \tag{8}$$

The *gauche* bonds can be classified as g^+ or g^- according to whether $\phi > \pi/3$ or $\phi < -\pi/3$. The distribution

$p(m)$ consists of two parts: the contribution from the *gauche* pairs with the same sign, $p_+(m)$, and that from the *gauche* pairs with the opposite sign, $p_-(m)$. The distribution $p(m)$ is then calculated by the sum of these two contributions: $p(m) = p_+(m) + p_-(m)$. The pair distribution functions $p_\pm(m)$ are shown in Fig. 7 at various times for $T = 400$ K. In the initial time region ($t = 0 \sim 50$ ps), no clear distinction can be observed between $p_+(m)$ and $p_-(m)$, and both of them decrease monotonically with the increase of the bond separation m [Fig. 7(a)]. There is no appreciable difference between $p_+(m)$ and $p_-(m)$ also in the time region of $t = 200 \sim 250$ ps, but the contributions from $m = 1$ and $m = 2$ become prominent [Fig. 7(b)]. In the next time region ($t = 250 \sim 300$ ps), notable difference between $p_+(m)$ and $p_-(m)$ can be seen for $m = 1$ and $m = 2$ [Fig. 7(c)]. For $m = 1$, the contribution from the *gauche* pairs with the same sign becomes marked. On the other hand, that from the *gauche* bonds with the opposite sign is dominant for $m = 2$. In the time region of $t = 1950 \sim 2000$ ps, the contributions from $m = 1$ and $m = 2$ become more and more conspicuous and those from $m \geq 3$, $p_\pm(m \geq 3)$, are all small [Fig. 7(d)]. This fact indicates that the *gauche* bonds tend to form small clusters. The fact that the contribution from the *gauche* bonds with the *same* sign is remarkable for $m = 1$ is in a striking contrast to the MD simulation results of a polymethylene chain confined in cylindrical potentials by Yamamoto *et al.*, where the contribution from $m = 1$ is very small for the *gauche* bonds both with the *same* sign and with the *opposite* sign [32]. They treated the system without free surfaces in their simulation. In our simulation, on the other hand, the system with free surfaces are dealt with. As we shall see later (Sec. 3.3.3), the contribution from the *gauche* bonds with the *same* sign for $m = 1$ mainly stems from the bonds on the free surface, that is, the end bonds in the outermost layer.

3.2.3 Parallel ordering

We investigate, in this subsection, the parallel ordering process. We first introduce the concept of a "*cluster*" as a bunch of local orientationally-ordered chain molecules which is formed through parallel ordering [20–22]. A cluster is defined in the following way. Two chain molecules belong to the same cluster if the following two conditions are satisfied: (i) $|\mathbf{r}_c^i - \mathbf{r}_c^j| < r_0$ and (ii) $\alpha_{ij} < \alpha_0$, where $\mathbf{r}_c^i$ is the position vector of the center of mass of the i-th chain molecule and α_{ij}, which satisfies $0 \leq \alpha_{ij} \leq \pi/2$, is the angle between the principal axis with the smallest moment of inertia of the i-th chain and that of the j-th chain. In our calculations, we set $r_0 = 1.5\sigma$ and $\alpha_0 = 10°$. We show, in Fig. 8, the time evolution of the largest cluster size s at $T = 400$ K. Up to $t \approx 120$ ps, only small clusters whose sizes are smaller than 10 can be observed. The largest cluster size s starts to increase sharply at $t \approx 120$ ps and grows in a stepwise fashion afterwards. A comparison made between the time evolution of $\overline{n_{\rm tr}}$ (Fig. 6) and that of s (Fig. 8) shows that parallel ordering of chain molecules starts to occur after the rigidity of chain molecules grows to some extent.

3.3 Molecular mobility and conformational defects in the orientationally ordered structure

3.3.1 Orientationally ordered structure

Here, we study the orientationally ordered structure at various temperatures. With a view to investigating the manner of lateral packing, we first calculate the two-dimensional (2D) radial distribution function for the center-of-mass positions of chain molecules in the a-b plane. The 2D radial distribution function $g_{\rm 2D}(r)$ averaged between 1500 ps and 2000 ps is shown in Fig. 9 at various temperatures. At $T \geq 200$ K, no remarkable difference can be found among the profiles of $g_{\rm 2D}(r)$. At $T = 100$ K, the first peak splits into two peaks and an additional peak appears between the second and the third peaks. The reason for this is that the equivalence between the direction of the a axis and that of the b axis breaks down as a result of the transition from the hexagonal phase toward the orthorhombic phase. We then calculate the lattice constants at various temperatures from the simulation data of the center-of-mass positions of chain molecules between 1500 ps and 2000 ps. In Fig. 10, the lattice constants a, b, and their ratio a/b are plotted as a function of temperature. Figures 10(a) and 10(b) indicates that the parameter a decreases with the decrease of temperature while the parameter b stays almost constant compared with the variation of a in this temperature region. From Fig. 10(c), it is found that chain molecules are packed hexagonally at $T = 400$K as mentioned above (see Fig. 2). The ratio a/b decreases as the temperature decreases, which indicates that the change from the hexagonal phase toward the orthorhombic phase takes place as the temperature decreases.

3.3.2 Translational motion

In this subsection, we investigate the translational motion of chain molecules at various temperatures. In order to measure the extent of the translational motion, we define the average fluctuations along individual axes in each layer l as

$$\Delta a(l) = \left\{ \sum_{m \in l\text{-th layer}} \frac{1}{n_l} \left\langle (a_{\rm c}^m - \langle a_{\rm c}^m \rangle)^2 \right\rangle \right\}^{1/2}, \quad (9)$$

$$\Delta b(l) = \left\{ \sum_{m \in l\text{-th layer}} \frac{1}{n_l} \left\langle (b_{\rm c}^m - \langle b_{\rm c}^m \rangle)^2 \right\rangle \right\}^{1/2}, \quad (10)$$

$$\Delta c(l) = \left\{ \sum_{m \in l\text{-th layer}} \frac{1}{n_l} \left\langle (c_{\rm c}^m - \langle c_{\rm c}^m \rangle)^2 \right\rangle \right\}^{1/2}, \quad (11)$$

where $\mathbf{r}_{\rm c}^m = (a_{\rm c}^m, b_{\rm c}^m, c_{\rm c}^m)$ is the position vector of the center of mass of the m-th chain molecule, n_l denotes the number of chain molecules involved in the l-th layer, $\langle \cdots \rangle$ represents the time average between 1500 ps and 2000 ps, and the zeroth layer means the central chain. In Fig. 11, we show the average fluctuations Δa, Δb and Δc as a function of the layer number l at various temperatures. This figure tells us that the longitudinal chain motion increases dramatically as the temperature increases [Fig. 11(c)] while the transverse chain motion is not so sensitive to the temperature variation [Figs. 11(a) and 11(b)]. At $T = 400$ K, the average longitudinal fluctuation Δc reaches about seven times the value of the average transverse fluctuation Δa or Δb. It is also found that both the transverse fluctuation and the longitudinal fluctuation increase remarkably in the outer three layers ($l = 4 \sim 6$) while they stay almost constant in the inner layers ($l = 0 \sim 3$). This result indicates that the chain molecules have much mobility in a few layers on the free surface. At $T \leq 300$K, the average longitudinal fluctuation Δc in the inner layers is smaller than $c/2 (= d_0 \cos(\theta_0/2) \approx 0.125$ nm), where c is the equilibrium lattice constant along the c axis. On the other hand, the fluctuation Δc becomes larger than $c/2$ even in the inner layers at $T = 400$K. It is quite understandable that the chain molecules can easily move in the longitudinal direction when the average longitudinal fluctuation Δc exceeds $c/2$. Considering that the chain molecules are packed hexagonally, we come to the conclusion that the chain molecules become longitudinally mobile in the case of hexagonal packing.

3.3.3 Conformational defects

As mentioned in Sec. 3.2.2 above, the contributions from the *gauche* pairs with the same sign for $m = 1$, $p_+(1)$, and from those with the opposite sign for $m = 2$, $p_-(2)$, are both remarkable. We here investigate what types of conformational defects contribute significantly to $p_+(1)$ and $p_-(2)$. Before calculating the fraction of several types of conformational defects which contribute to $p_+(1)$ and $p_-(2)$, we prescribe the types of conformational defects. We define the following four types of conformational defects: double *gauche*, triple *gauche*, kink and coupled kink. Details of these conformational defects are explained in Table 3. The symbols DG1 and DG2 respectively denote double *gauche* defects composed of the *gauche* pairs with the *same* sign and with the *opposite* sign. Triple *gauche* defects are classified into three groups: TG1, TG2 and TG3. Among these conformational defects, DG1, TG1 and TG2 contribute to $p_+(1)$, and TG2, K and CK to $p_-(2)$. We show, in Fig. 12, the average fraction of the conformational defects between 1500 ps and 2000 ps which contribute to $p_+(1)$ and $p_-(2)$ at $T = 400$ K. This figure tells us that the *gauche* pairs with the same sign tend to form the double *gauche* defects (DG1) and those with the opposite sign tend to form the kink defects (K). The latter result is also observed in the above-mentioned MD simulation by Yamamoto *et al.* [32].

We then study the spatial distribution of the double *gauche* defects (DG1) and the kink defects (K). The spatial distribution function $P(n_{\rm D}, l)$ is normalized as

$$\sum_{n_{\rm D}=1}^{n_{\rm D}^{\rm max}} \sum_{l=0}^{l_{\rm max}} \frac{1}{n_l} P(n_{\rm D}, l) = 1, \quad (12)$$

where $n_{\rm D}$ denotes the defect number along the chain molecule, $l_{\rm max}$ represents the maximum layer number ($l_{\rm max} = 6$ in our case), and $n_{\rm D}^{\rm max}$ is the maximum defect number ($n_{\rm D}^{\rm max} = 16$ for DG1 and $n_{\rm D}^{\rm max} = 15$ for K). Note that the conformational defects with $n_{\rm D} = 1$ and $n_{\rm D} = n_{\rm D}^{\rm max}$ correspond to the end defects. The spatial distribution function $P(n_{\rm D}, l)$ averaged between 1500 ps and 2000 ps is shown in Fig. 13 as a function of $n_{\rm D}$ and l for DG1 and K at $T = 400$ K. It is found from Fig. 13(a) that the double *gauche* defects (DG1) are predominantly located at the chain ends in the outermost layer. This can be understood in the following way. When the double *gauche* defects (DG1) are located in the chain interiors, chain molecules are prevented from packing laterally because of large deformation of chain molecules. Thus the energy loss due to the double *gauche* defects (DG1) located in the chain interiors becomes large. When the defects are located in the outermost layer, the energy loss due to the appearance of the defects (DG1) is considered to be small since the outermost layer is a free surface where the constraint by surrounding chain molecules is weak. Therefore the double *gauche* defects (DG1) tend to locate at the chain ends in the outermost layer. Figure 13(b) tells us that most of the kink defects are located in the outermost layer. In contrast to the double *gauche* defects (DG1), the kink defects does not give rise to serious deformation of chain molecules even in the chain interiors. Therefore the energy loss is small even though the kink defects are located in the chain interiors.

4 Summary and Discussion

In this paper, we have carried out MD simulations of short chain-molecule systems with free surfaces. By analyzing the microscopic processes of the structure formation and investigating the molecular mobility and the conformational defects in the obtained orientationally-ordered structure, the following results have been obtained:

(1) The orientationally ordered structure is formed at low temperature from a random configuration at high temperature by quenching.

(2) The global orientational order sharply starts to grow after a certain initial duration.
(3) The fraction of the *trans* states increases even in the initial duration when no global orientational order exists.
(4) The rigidity of chain molecules starts to grow as the transition from the *gauche* state to the *trans* state proceeds. The rigidity of chain molecules starts to grow before the parallel ordering starts to proceed.
(5) Both the largest cluster size and the global orientational order grow in a stepwise fashion.
(6) The chain molecules are packed hexagonally at $T = 400$ K. The transition from the hexagonal phase toward the orthorhombic phase takes place as the temperature decreases.
(7) The longitudinal chain motion increases dramatically as the temperature increases. The chain molecules in a few layers on the free surface have much mobility. In the hexagonal phase, the average longitudinal fluctuation Δc becomes larger than $c/2$ even in the inner layers, which means that the chain molecules become longitudinally mobile in the case of hexagonal packing.
(8) The *gauche* bonds in the same chain molecule tend to form *gauche* pairs. The *gauche* pairs with the same sign form the double *gauche* defects and those with the opposite sign form the kink defects. The double *gauche* defects with the same sign are predominantly located at the chain ends in the outermost layer and most of the kink defects are located in the outermost layer.

Our conclusion that the chain molecules become longitudinally mobile in the hexagonal phase is drawn by the microscopic analysis of the chain motion. Therefore this conclusion is the microscopic evidence to confirm the existence of the chain sliding diffusion in the hexagonal phase which underlies the sliding diffusion theory of polymer crystallization proposed by Hikosaka [33,34]. The chain sliding diffusion is the sliding motion along the chain axes of chain molecules within crystals or nuclei, or crystal/melt interfaces. Since the chain sliding diffusion occurs readily in the hexagonal phase, extended chain crystals are formed through the lamellar thickening growth. On the other hand, folded chain crystals are formed in the orthorhombic phase because the chain sliding diffusion is hindered and accordingly the lamellar thickening growth is suppressed.

In our simulation, the orientationally-ordered structure is formed at the temperature above the bulk freezing point of n-$C_{20}H_{42}$ ($T_f \approx 38°C$). This observation is similar to the surface freezing phenomenon which is observed on the free surface of liquid n-alkanes a few degrees above their freezing temperatures. There are several reasons why the ordered structure is formed far above the freezing temperature in our simulation. One is that the obtained structure is a monolayer structure. Another reason is that the torsional energy difference between the *trans* and the *gauche* states in the DREIDING potential is larger than that in the real n-alkanes.

Molecular dynamics simulations of long chain molecules are under way in order to investigate the effect of the entanglement on the structure formation.

Acknowledgments

This work was partially supported by a Grant-in-Aid for Scientific Research on Priority Areas, Cooperative Phenomena in Complex Liquids, from the Ministry of Education, Science, Sports and Culture. This work was carried out by using the Advanced Computing System for Complexity Simulation (NEC SX-3/24R) at National Institute for Fusion Science.

References

[1] M. Hikosaka, S. Rastogi, A. Keller and H. Kawabata, J. Macromol. Sci. Phys. B **31**, 87 (1992) and references therein.

[2] A. Keller, M. Hikosaka, S. Rastogi, A. Toda, P.J. Barham and G. Goldbeck-Wood, J. Mater. Sci. **29**, 2579 (1994).

[3] K. Tashiro, M. Izuchi, F. Kaneuchi, C. Jin, M. Kobayashi and R.S. Stein, Macromolecules **27**, 1240 (1994).

[4] K. Tashiro, K. Imanishi, Y. Izumi, M. Kobayashi, K. Kobayashi, M. Satoh and R.S. Stein, Macromolecules **28**, 8477 (1995).

[5] K. Tashiro, S. Sasaki and M. Kobayashi, Macromolecules **29**, 7460 (1996).

[6] M. Imai, K. Kaji and T. Kanaya, Phys. Rev. Lett. **71**, 4162 (1993).

[7] M. Imai, K. Kaji and T. Kanaya, Macromolecules **27**, 7103 (1994).

[8] M. Imai, K. Kaji, T. Kanaya and Y. Sakai, Physica B **213/214**, 718 (1995).

[9] M. Imai, K. Kaji, T. Kanaya and Y. Sakai, Phys. Rev. B **52**, 12696 (1995).

[10] K. Fukao and Y. Miyamoto, Phys. Rev. Lett. **79**, 4613 (1997).

[11] K. Fukao and Y. Miyamoto, J. Non-Cryst. Solids **212**, 208 (1997).

[12] J.C. Earnshaw and C.J. Hughes, Phys. Rev. A **46**, R4494 (1992).

[13] X.Z. Wu, E.B. Sirota, S.K. Sinha, B.M. Ocko and M. Deutsch, Phys. Rev. Lett. **70**, 958 (1993).

[14] X.Z. Wu, B.M. Ocko, E.B. Sirota, S.K. Sinha, M. Deutsch, B.H. Cao and M.W. Kim, Science **261**, 1018 (1993).

[15] X.Z. Wu, B.M. Ocko, H. Tang, E.B. Sirota, S.K. Sinha and M. Deutsch, Phys. Rev. Lett. **75**, 132 (1995).

[16] M. Deutsch, X.Z. Wu, E.B. Sirota, S.K. Sinha, B.M. Ocko and O.M. Magnussen, Europhys. Lett. **30**, 283 (1995).

[17] T.A. Kavassalis and P.R. Sundararajan, Macromolecules **26**, 4144 (1993).

[18] P.R. Sundararajan and T.A. Kavassalis, J. Chem. Soc. Faraday Trans. **91**, 2541 (1995).

[19] S. Fujiwara and T. Sato, J. Chem. Phys. **107**, 613 (1997).

[20] K. Esselink, P.A.J. Hilbers and B.W.H. van Beest, J. Chem. Phys. **101**, 9033 (1994).

[21] S. Fujiwara and T. Sato, Phys. Rev. Lett. **80**, 991 (1998).

[22] S. Fujiwara and T. Sato, Molecular Simulation (in press).

[23] H. Takeuchi, J. Chem. Phys. **109**, 5614 (1998).

[24] M. Kawamata and T. Yamamoto, J. Phys. Soc. Jpn. **66**, 2350 (1997).

[25] T. Yamamoto, J. Chem. Phys. **107**, 2653 (1997).

[26] T. Yamamoto, J. Chem. Phys. **109**, 4638 (1998).

[27] S.L. Mayo, B.D. Olafson and W.A. Goddard III, J. Phys. Chem. **94**, 8897 (1990).

[28] L. Verlet, Phys. Rev. **159**, 98 (1967).

[29] S. Nosé, Mol. Phys. **52**, 255 (1984).

[30] S. Nosé, J. Chem. Phys. **81**, 511 (1984).

[31] W.G. Hoover, Phys. Rev. A **31**, 1695 (1985).

[32] T. Yamamoto and Y. Kimikawa, J. Chem. Phys. **97**, 5163 (1992).

[33] M. Hikosaka, Polymer **28**, 1257 (1987).

[34] M. Hikosaka, Polymer **31**, 458 (1990).

Table 1: Potential energy parameters used in our simulation [27].

parameter	value	unit
d_0	0.153	nm
θ_0	1.2310	rad
k_d	70000	kcal/nm^2·mol
k_θ	100	kcal/rad^2·mol
k_φ	2.0	kcal/mol
ϵ	0.1984	kcal/mol
σ	0.36239	nm

Table 2: The average number of *gauche* bonds n_G, isolated *gauche* bonds n_IG and their ratio $n_\mathrm{IG}/n_\mathrm{G}$ in each time interval at $T = 400$ K.

time (ps)	n_G	n_IG	$n_\mathrm{IG}/n_\mathrm{G}$
0∼500	73.87	25.39	0.344
500∼1000	29.23	17.92	0.613
1000∼1500	25.37	16.64	0.656
1500∼2000	23.76	15.92	0.670

Table 3: Explanation of four types of conformational defects: double *gauche*, triple *gauche*, kink and coupled kink. In the column of "example", 't' and 'g$^\pm$' denote the *trans* and the *gauche* states, respectively.

type	symbol	example
double *gauche*	DG1	$\cdots$tg$^+$g$^+$t$\cdots$, $\cdots$tg$^-$g$^-$t$\cdots$
	DG2	$\cdots$tg$^+$g$^-$t$\cdots$
triple *gauche*	TG1	$\cdots$tg$^+$g$^+$g$^+$t$\cdots$, $\cdots$tg$^-$g$^-$g$^-$t$\cdots$
	TG2	$\cdots$tg$^+$g$^+$g$^-$t$\cdots$, $\cdots$tg$^-$g$^-$g$^+$t$\cdots$
	TG3	$\cdots$tg$^+$g$^-$g$^+$t$\cdots$, $\cdots$tg$^-$g$^+$g$^-$t$\cdots$
kink	K	$\cdots$tg$^+$tg$^-$t$\cdots$
coupled kink	CK	$\cdots$tg$^+$tg$^-$tg$^+$t$\cdots$, $\cdots$tg$^-$tg$^+$tg$^-$t$\cdots$

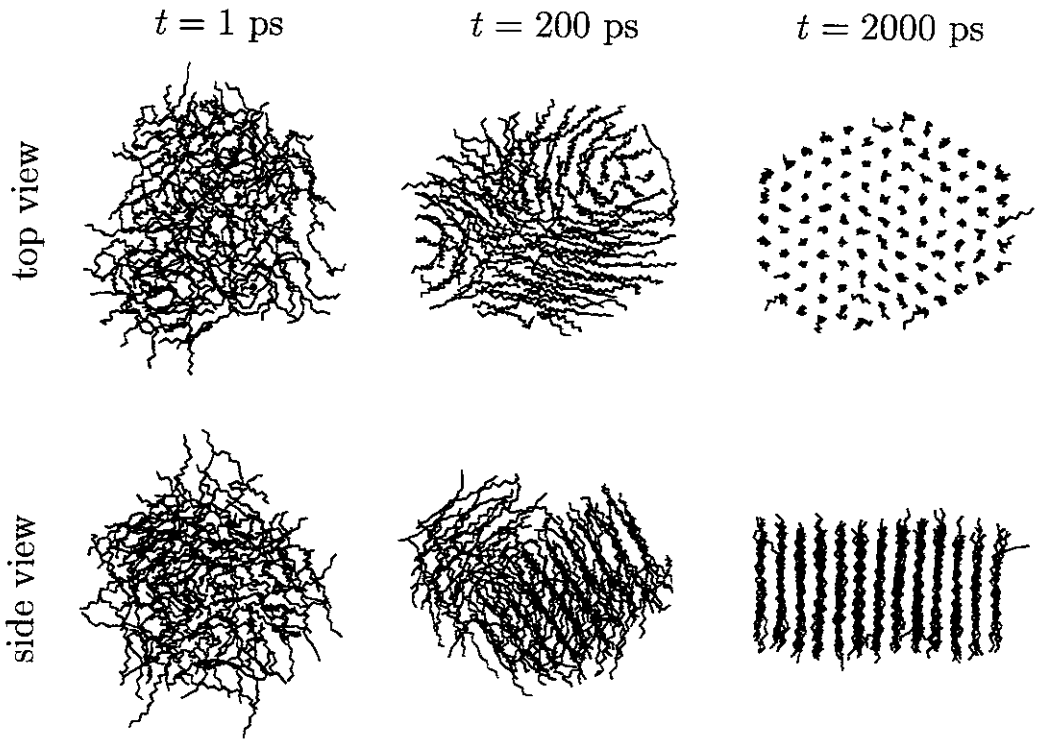

Figure 1: Snapshots of the chain configuration of 100 short chain molecules at various times: $t = 1$ ps, 200 ps and 2000 ps (from left to right) for $T = 400$ K. Top and bottom figures are respectively viewed along the c axis (top view) and the b axis (side view).

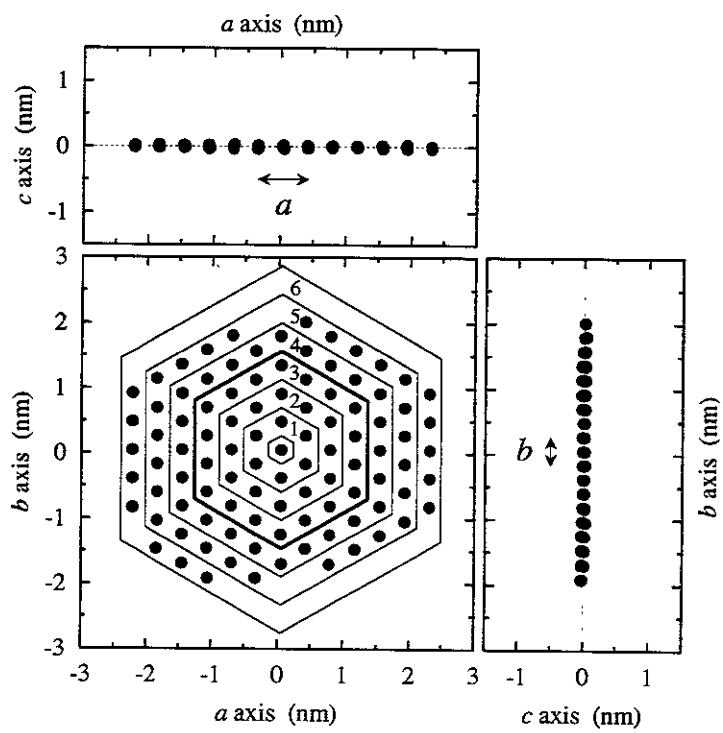

Figure 2: The center-of-mass positions of individual chain molecules viewed along the a, b and c axes averaged between 1500 ps and 2000 ps for $T = 400$ K. The lattice constants a and b are $a = 0.750$ nm and $b = 0.433$ nm, respectively. Hexagons are depicted in order to show a hexagonal packing of the chain molecules. A figure in each layer represents a layer number l. The a, b and c axes are determined by the central 37 chains within a thick hexagon.

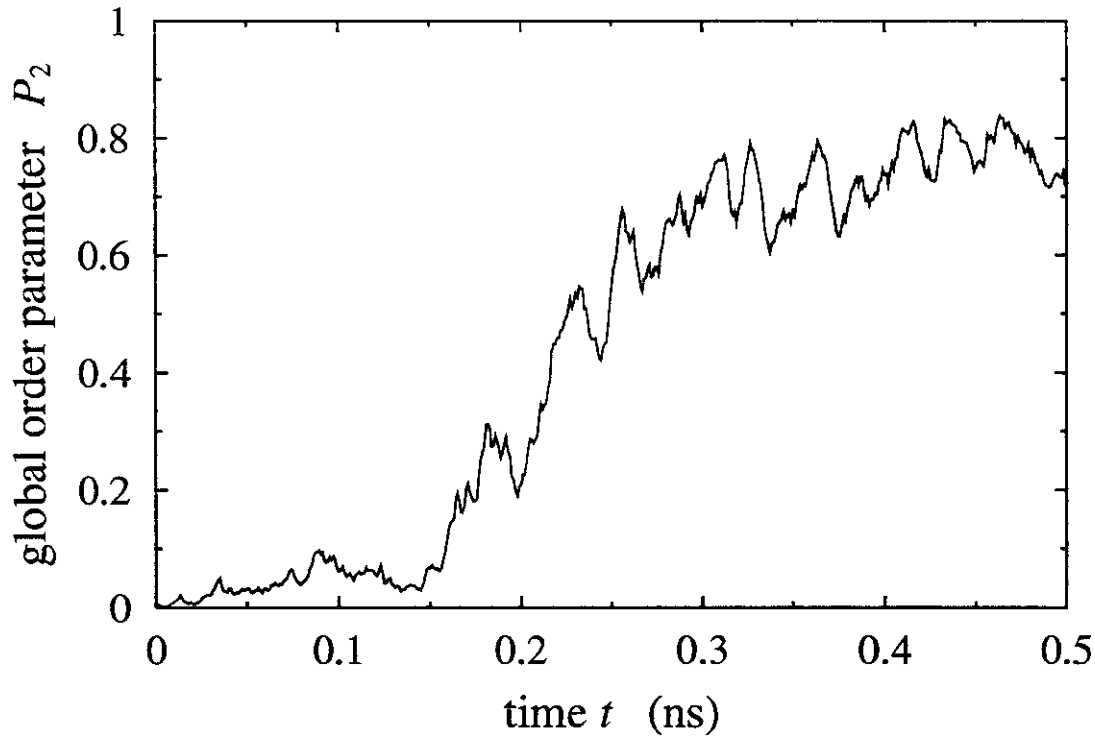

Figure 3: The global orientational order parameter P_2 vs. time t at $T = 400$ K.

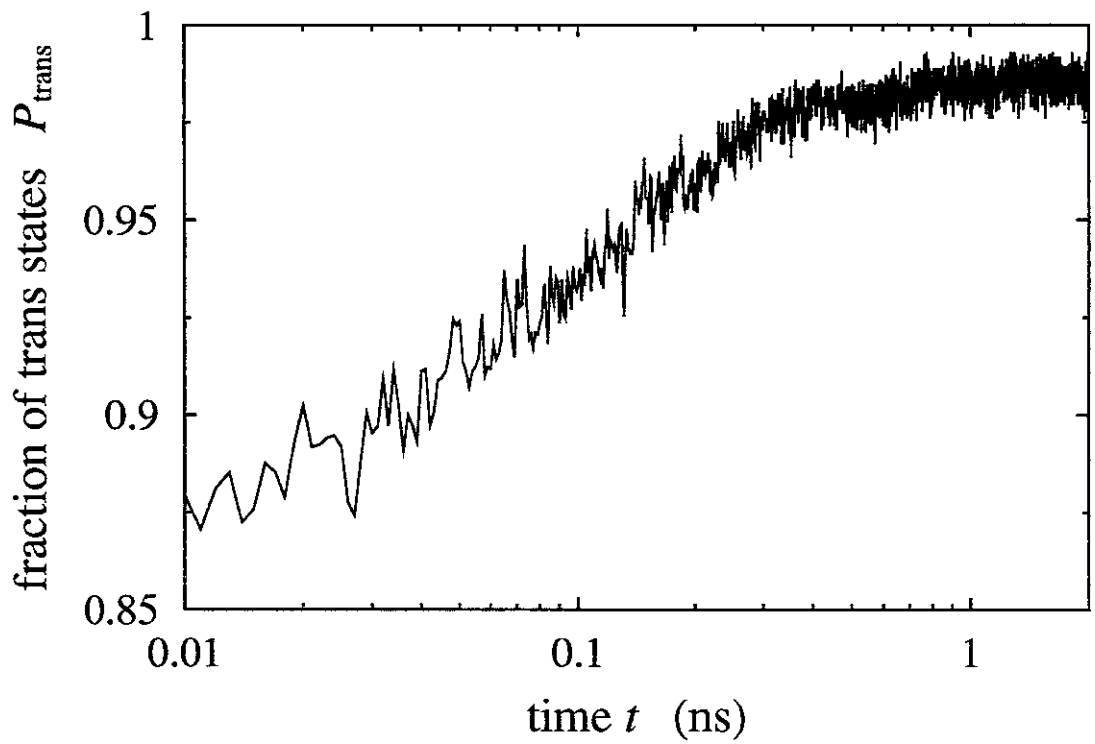

Figure 4: The fraction of the *trans* states P_{trans} vs. time t at $T = 400$ K.

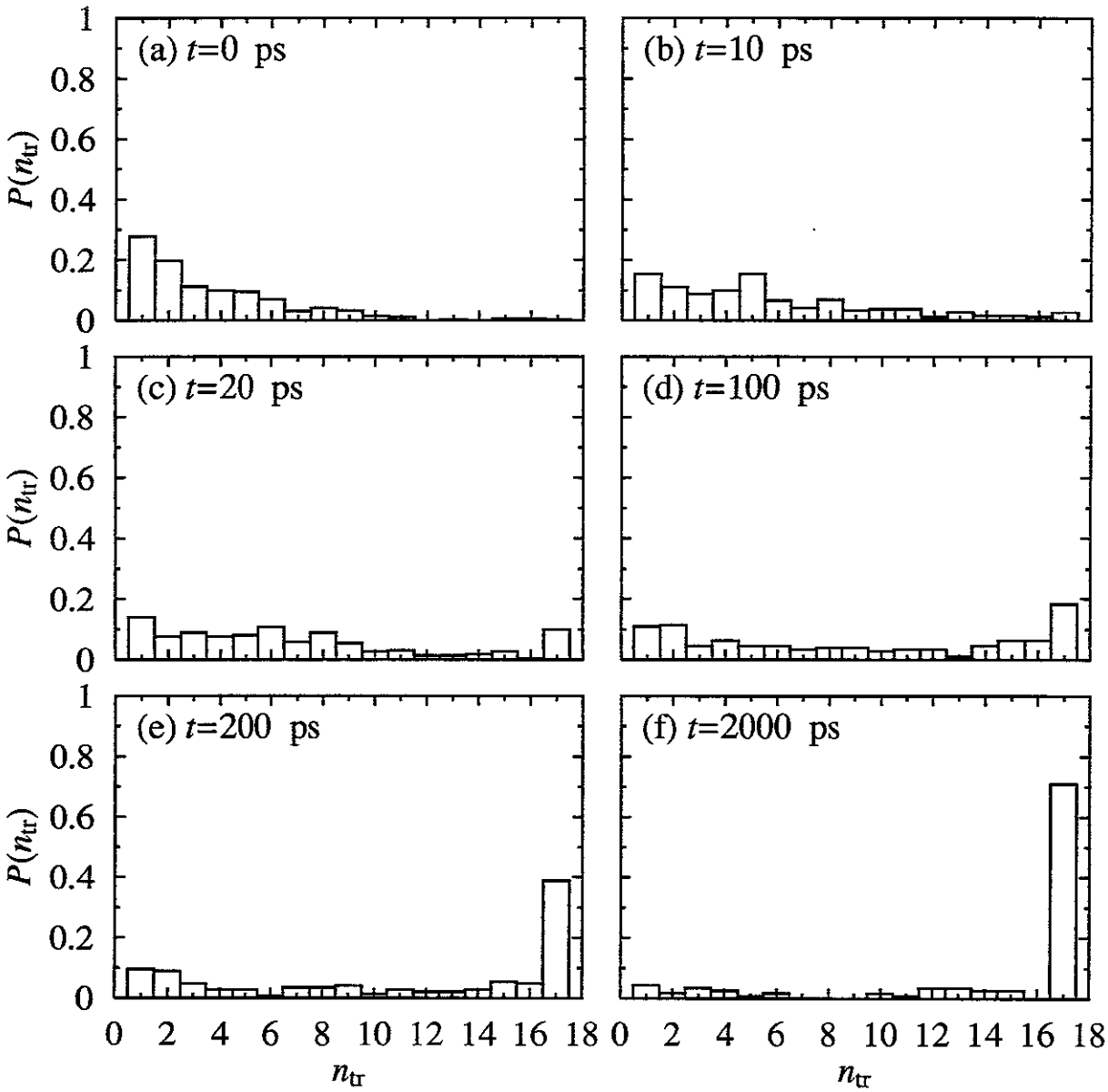

Figure 5: The distribution of the size of the *trans* segments $P(n_{\rm tr})$ for $T = 400$ K at various times: (a) 0 ps, (b) 10 ps, (c) 20 ps, (d) 100 ps, (e) 200 ps and (f) 2000 ps.

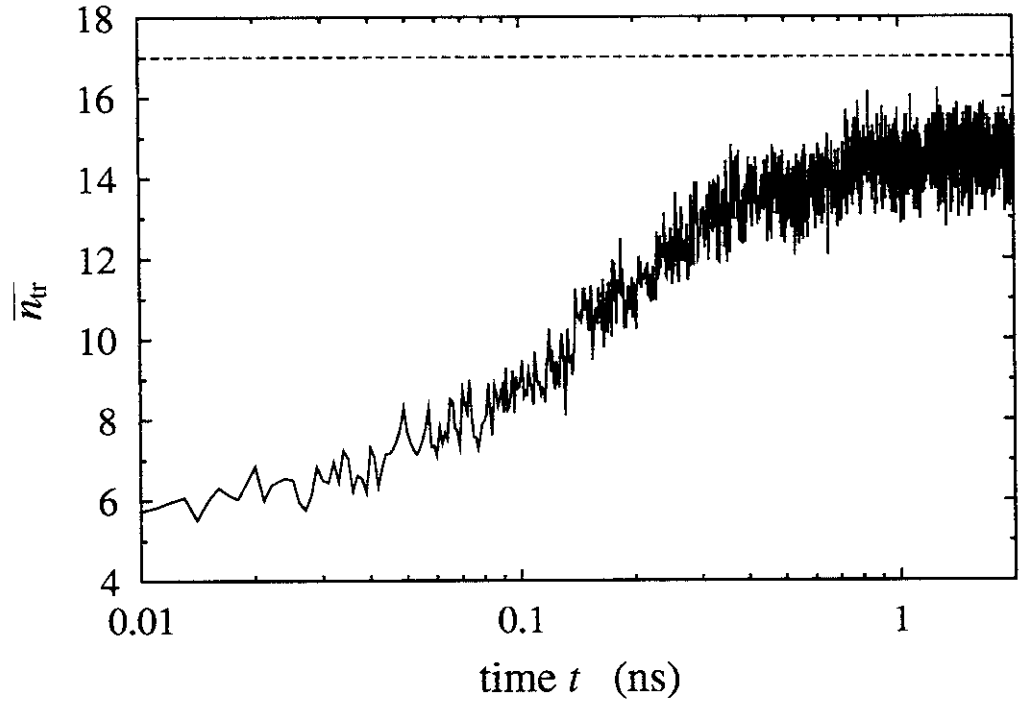

Figure 6: The average size of the *trans* segments $\overline{n_{\rm tr}}$ vs. time t at $T = 400$ K. The dashed line represents the upper limit of $\overline{n_{\rm tr}}$.

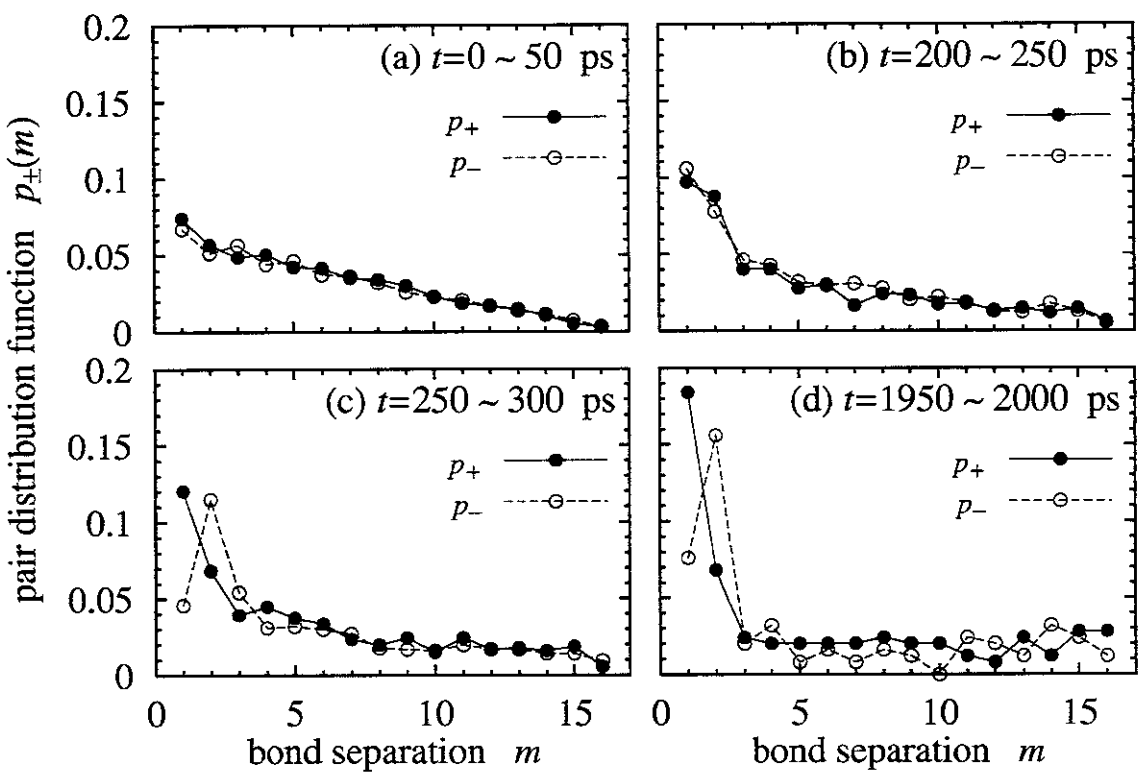

Figure 7: The pair distribution function $p_\pm(m)$ vs. bond separation m for $T = 400$ K at various time intervals: (a) 0~50 ps, (b) 200~250 ps, (c) 250~300 ps and (d) 1950~2000 ps.

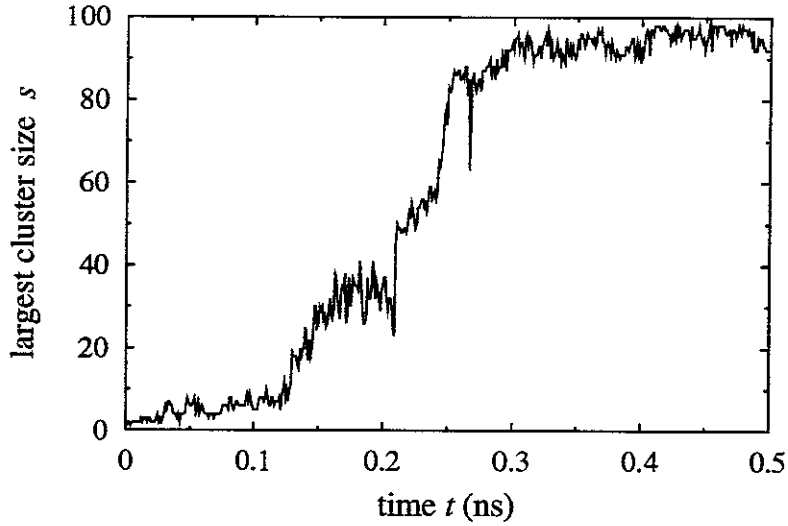

Figure 8: The largest cluster size s vs. time t at $T = 400$ K.

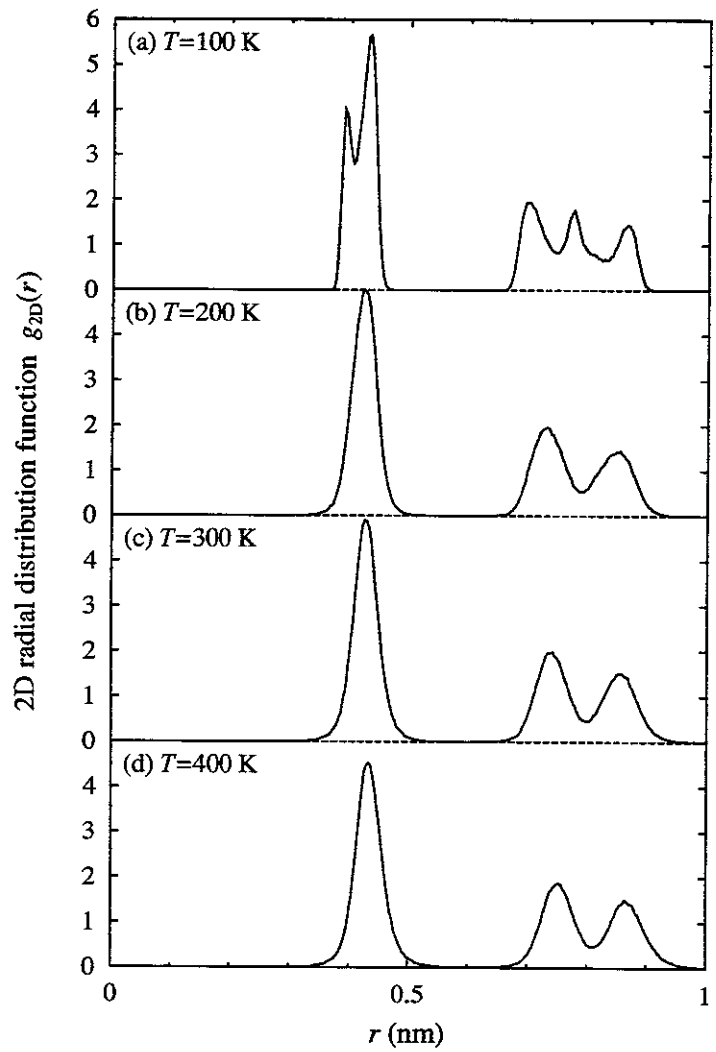

Figure 9: The 2D radial distribution function $g_{2D}(r)$ averaged between 1500 ps and 2000 ps at various temperatures: (a) $T = 100$ K, (b) $T = 200$ K, (c) $T = 300$ K and (d) $T = 400$ K.

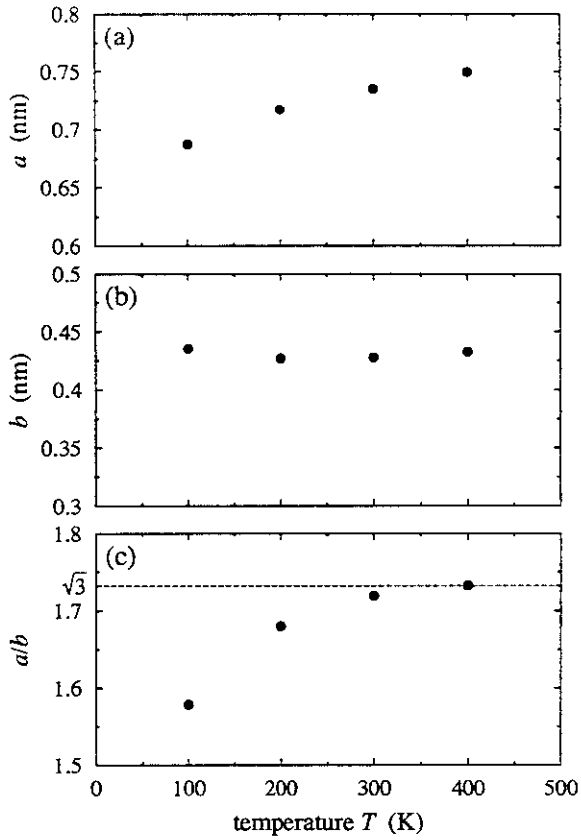

Figure 10: Lattice constants (a) a, (b) b and (c) the ratio a/b vs. temperature T. A dashed line in (c) indicates the hexagonal value $\sqrt{3}$.

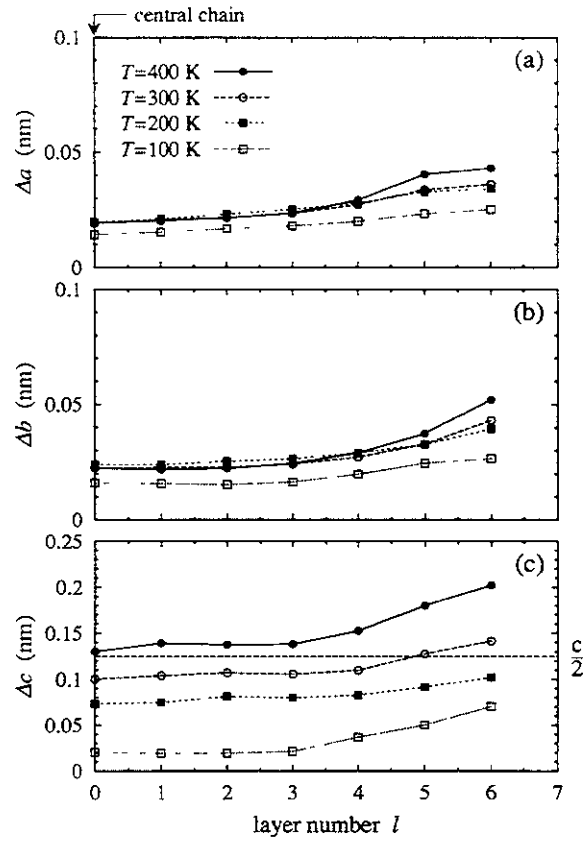

Figure 11: Average fluctuations (a) along the a axis Δa, (b) along the b-axis Δb and (c) along the c-axis Δc vs. layer number l at various temperatures. A dashed line in (c) indicates $c/2$, where c is the equilibrium lattice constant along the c axis.

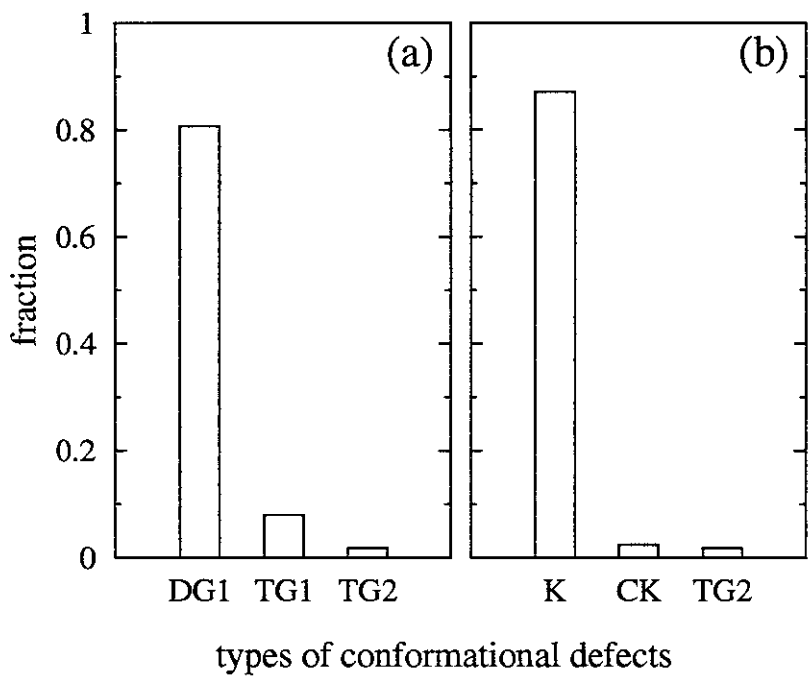

Figure 12: The fraction of the conformational defects averaged between 1500 ps and 200 ps which contribute (a) to $p_+(1)$ and (b) to $p_-(2)$ at $T = 400$ K. Symbols such as DG1 and TG1 are explained in Table ??.

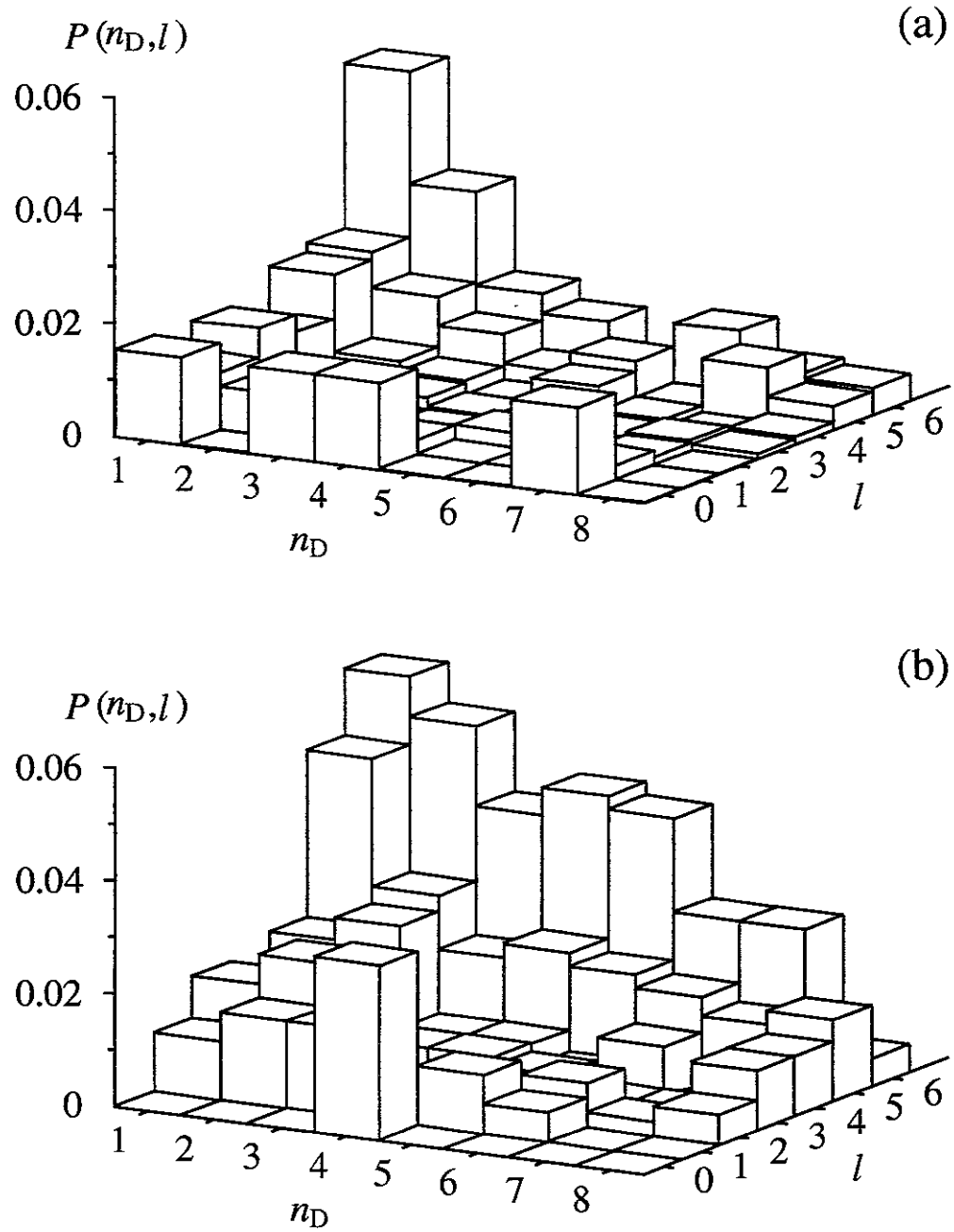

Figure 13: The average spatial distribution function $P(n_D, l)$ between 1500 ps and 200 ps as a function of n_D and l (a) for DG1 and (b) for K at $T = 400$ K.

Recent Issues of NIFS Series

NIFS-513 T Shimozuma, M Sato, Y Takita, S Ito, S Kubo, H Idei, K Ohkubo, T Watari, T S Chu, K Felch P Cahalan and C M Loring, Jr,
The First Preliminary Experiments on an 84 GHz Gyrotron with a Single-Stage Depressed Collector, Oct 1997

NIFS-514 T Shimozuma, S Morimoto, M. Sato, Y Takita, S Ito, S Kubo, H Idei, K Ohkubo and T Watari,
A Forced Gas-Cooled Single-Disk Window Using Silicon Nitride Composite for High Power CW Millimeter Waves, Oct 1997

NIFS-515 K Akaishi,
On the Solution of the Outgassing Equation for the Pump down of an Unbaked Vacuum System; Oct 1997

NIFS-516 *Papers Presented at the 6th H-mode Workshop (Seeon, Germany)*; Oct 1997

NIFS-517 John L. Johnson,
The Quest for Fusion Energy, Oct 1997

NIFS-518 J Chen, N Nakajima and M. Okamoto,
Shift-and-Inverse Lanczos Algorithm for Ideal MHD Stability Analysis, Nov. 1997

NIFS-519 M Yokoyama, N. Nakajima and M Okamoto,
Nonlinear Incompressible Poloidal Viscosity in L=2 Heliotron and Quasi-Symmetric Stellarators, Nov. 1997

NIFS-520 S Kida and H Miura,
Identification and Analysis of Vortical Structures, Nov 1997

NIFS-521 K. Ida, S Nishimura, T. Minami, K. Tanaka, S Okamura, M Osakabe, H. Idei, S Kubo, C Takahashi and K Matsuoka,
High Ion Temperature Mode in CHS Heliotron/torsatron Plasmas; Nov. 1997

NIFS-522 M Yokoyama, N. Nakajima and M. Okamoto,
Realization and Classification of Symmetric Stellarator Configurations through Plasma Boundary Modulations; Dec 1997

NIFS-523 H Kitauchi,
Topological Structure of Magnetic Flux Lines Generated by Thermal Convection in a Rotating Spherical Shell; Dec. 1997

NIFS-524 T. Ohkawa,
Tunneling Electron Trap, Dec 1997

NIFS-525 K Itoh, S.-I. Itoh, M Yagi, A Fukuyama,
Solitary Radial Electric Field Structure in Tokamak Plasmas, Dec 1997

NIFS-526 Andrey N. Lyakhov,
Alfven Instabilities in FRC Plasma; Dec 1997

NIFS-527 J. Uramoto,
Net Current Increment of negative Muonlike Particle Produced by the Electron and Positive Ion Bunch-method; Dec 1997

NIFS-528 Andrey N Lyakhov,
Comments on Electrostastic Drift Instabilities in Field Reversed Configuraiton, Dec 1997

NIFS-529 J. Uramoto,
Pair Creation of Negative and Positive Pionlike (Muonlike) Particle by Interaction between an Electron Bunch and a Positive Ion Bunch; Dec 1997

NIFS-530 J. Uramoto,
Measuring Method of Decay Time of Negative Muonlike Particle by Beam Collector Applied RF Bias Voltage, Dec. 1997

NIFS-531 J. Uramoto,

Confirmation Method for Metal Plate Penetration of Low Energy Negative Pionlike or Muonlike Particle Beam under Positive Ions; Dec. 1997

NIFS-532 J. Uramoto,
Pair Creations of Negative and Positive Pionlike (Muonlike) Particle or K Mesonlike (Muonlike) Particle in H2 or D2 Gas Discharge in Magnetic Field; Dec. 1997

NIFS-533 S. Kawata, C. Boonmee, T Teramoto, L. Drska, J Limpouch, R. Liska, M. Sinor,
Computer-Assisted Particle-in-Cell Code Development; Dec 1997

NIFS-534 Y. Matsukawa, T. Suda, S. Ohnuki and C. Namba,
Microstructure and Mechanical Property of Neutron Irradiated TiNi Shape Memory Alloy; Jan 1998

NIFS-535 A. Fujisawa, H Iguchi, H. Idei, S. Kubo, K. Matsuoka, S Okamura, K. Tanaka, T. Minami, S Ohdachi, S Monta, H Zushi, S. Lee, M. Osakabe, R. Akiyama, Y Yoshimura, K Toi, H. Sanuki, K. Itoh, A. Shimizu, S. Takagi, A. Ejiri, C Takahashi, M. Kojima, S Hidekuma, K Ida, S Nishimura, N. Inoue, R. Sakamoto, S.-I. Itoh, Y. Hamada, M. Fujiwara,
Discovery of Electric Pulsation in a Toroidal Helical Plasma; Jan. 1998

NIFS-536 Lj.R. Hadzievski, M.M. Skoric, M. Kono and T. Sato,
Simulation of Weak and Strong Langmuir Collapse Regimes; Jan. 1998

NIFS-537 H. Sugama, W. Horton,
Nonlinear Electromagnetic Gyrokinetic Equation for Plasmas with Large Mean Flows, Feb. 1998

NIFS-538 H. Iguchi, T P. Crowley, A. Fujisawa, S Lee, K. Tanaka, T. Minami, S. Nishimura, K Ida, R Akiyama, Y Hamada, H , Idei M. Isobe, M. Kojima, S. Kubo, S. Monta, S. Ohdachi, S Okamura, M Osakabe, K Matsuoka, C. Takahashi and K. Toi,
Space Potential Fluctuations during MHD Activities in the Compact Helical System (CHS); Feb. 1998

NIFS-539 Takashi Yabe and Yan Zhang,
Effect of Ambient Gas on Three-Dimensional Breakup in Coronet Formation Process; Feb. 1998

NIFS-540 H. Nakamura, K. Ikeda and S. Yamaguchi,
Transport Coefficients of InSb in a Strong Magnetic Field, Feb. 1998

NIFS-541 J. Uramoto,
Development of ν_μ Beam Detector and Large Area ν_μ Beam Source by H_2 Gas Discharge (I); Mar. 1998

NIFS-542 J. Uramoto,
Development of $bar\{\nu\}_\mu$ Beam Detector and Large Area $bar\{\nu\}_\mu$ Beam Source by H_2 Gas Discharge (II), Mar. 1998

NIFS-543 J. Uramoto,
Some Problems inside a Mass Analyzer for Pions Extracted from a H_2 Gas Discharge, Mar 1998

NIFS-544 J Uramoto,
Simplified ν_μ, $bar\{\nu\}_\mu$ Beam Detector and ν_μ, $bar\{\nu\}_\mu$ Beam Source by Interaction between an Electron Bunch and a Positive Ion Bunch; Mar. 1998

NIFS-545 J Uramoto,
Various Neutrino Beams Generated by D_2 Gas Discharge; Mar 1998

NIFS-546 R. Kanno, N. Nakajima, T Hayashi and M Okamoto,
Computational Study of Three Dimensional Equilibria with the Bootstrap Current; Mar 1998

NIFS-547 R. Kanno, N. Nakajima and M. Okamoto,
Electron Heat Transport in a Self-Similar Structure of Magnetic Islands; Apr. 1998

NIFS-548 J.E. Rice,
Simulated Impurity Transport in LHD from MIST; May 1998

NIFS-549 M.M. Skoric, T. Sato, A.M. Maluckov and M.S. Jovanovic,
On Kinetic Complexity in a Three-Wave Interaction; June 1998

NIFS-550 S Goto and S Kida,
Passive Scalar Spectrum in Isotropic Turbulence: Prediction by the Lagrangian Direct-interaction Approximation; June 1998

NIFS-551 T Kuroda, H Sugama, R Kanno, M Okamoto and W Horton,
Initial Value Problem of the Toroidal Ion Temperature Gradient Mode, June 1998

NIFS-552 T Mutoh, R Kumazawa, T Seki, F Simpo, G Nomura, T Ido and T Watari,
Steady State Tests of High Voltage Ceramic Feedthroughs and Co-Axial Transmission Line of ICRF Heating System for the Large Helical Device; June 1998

NIFS-553 N Noda, K. Tsuzuki, A Sagara, N Inoue, T Muroga,
oronization in Future Devices -Protecting Layer against Tritium and Energetic Neutrals-, July 1998

NIFS-554 S Murakami and H Saleem,
Electromagnetic Effects on Rippling Instability and Tokamak Edge Fluctuations; July 1998

NIFS-555 H Nakamura, K Ikeda and S Yamaguchi,
Physical Model of Nernst Element, Aug 1998

NIFS-556 H Okumura, S Yamaguchi, H Nakamura, K Ikeda and K Sawada
Numerical Computation of Thermoelectric and Thermomagnetic Effects, Aug 1998

NIFS-557 Y Takeiri, M. Osakabe, K Tsumori, Y Oka, O Kaneko, E Asano, T Kawamoto, R. Akiyama and M Tanaka,
Development of a High-Current Hydrogen-Negative Ion Source for LHD-NBI System, Aug 1998

NIFS-558 M. Tanaka, A Yu Grosberg and T Tanaka,
Molecular Dynamics of Structure Organization of Polyampholytes, Sep 1998

NIFS-559 R Horiuchi, K. Nishimura and T Watanabe,
Kinetic Stabilization of Tilt Disruption in Field-Reversed Configurations, Sep 1998
(IAEA-CN-69/THP1/11)

NIFS-560 S Sudo, K Kholopenkov, K Matsuoka, S Okamura, C Takahashi, R Akiyama, A. Fujisawa, K Ida, H. Idei, H Iguchi, M Isobe, S Kado, K Kondo, S. Kubo, H Kuramoto, T Minami, S Morita, S Nishimura, M Osakabe, M Sasao, B Peterson, K Tanaka, K Toi and Y Yoshimura,
Particle Transport Study with Tracer-Encapsulated Solid Pellet Injection, Oct 1998
(IAEA-CN-69/EXP1/18)

NIFS-561 A Fujisawa, H. Iguchi, S Lee, K Tanaka, T Minami, Y Yoshimura, M Osakabe, K Matsuoka, S Okamura, H Idei, S Kubo, S Ohdachi, S. Morita, R. Akiyama, K. Toi, H Sanuki, K Itoh, K. Ida, A Shimizu, S Takagi, C. Takahashi, M. Kojima, S Hidekuma, S Nishimura, M Isobe, A. Ejiri, N Inoue, R. Sakamoto, Y Hamada and M. Fujiwara,
Dynamic Behavior Associated with Electric Field Transitions in CHS Heliotron/Torsatron, Oct 1998
(IAEA-CN-69/EX5/1)

NIFS-562 S. Yoshikawa,
Next Generation Toroidal Devices; Oct 1998

NIFS-563 Y Todo and T Sato,
Kinetic-Magnetohydrodynamic Simulation Study of Fast Ions and Toroidal Alfvén Eigenmodes; Oct 1998
(IAEA-CN-69/THP2/22)

NIFS-564 T. Watari, T. Shimozuma, Y Takeiri, R Kumazawa, T Mutoh, M Sato, O Kaneko, K. Ohkubo, S. Kubo, H Idei, Y Oka, M. Osakabe, T Seki, K Tsumori, Y. Yoshimura, R Akiyama, T Kawamoto, S Kobayashi, F Shimpo, Y Takita, E Asano S Itoh, G Nomura, T. Ido, M Hamabe, M. Fujiwara, A Iiyoshi, S Morimoto, T Bigelow and Y P Zhao,
Steady State Heating Technology Development for LHD, Oct 1998
(IAEA-CN-69/FTP/21)

NIFS-565 A Sagara, K Y. Watanabe, K Yamazaki, O Motojima, M Fujiwara, O Mitarai, S. Imagawa, H. Yamanishi, H Chikaraishi, A. Kohyama, H. Matsui, T Muroga, T Noda, N Ohyabu, T Satow, A A Shishkin, S Tanaka, T Terai and T Uda,
LHD-Type Compact Helical Reactors; Oct 1998
(IAEA-CN-69/FTP/03(R)

NIFS-566 N Nakajima, J Chen, K Ichiguchi and M Okamoto,
Global Mode Analysis of Ideal MHD Modes in L=2 Heliotron/Torsatron Systems, Oct 1998
(IAEA-CN-69/THP1/08)

NIFS-567 K Ida, M. Osakabe, K. Tanaka, T. Minami, S. Nishimura, S. Okamura, A. Fujisawa, Y Yoshimura, S Kubo, R. Akiyama, D.S Darrow, H Idei, H. Iguchi, M Isobe, S Kado, T. Kondo, S. Lee, K. Matsuoka, S Morita, I Nomura, S. Ohdachi, M. Sasao, A Shimizu, K. Tumon, S. Takayama, M. Takechi, S Takagi, C. Takahashi, K. Toi and T. Watari,
Transition from L Mode to High Ion Temperature Mode in CHS Heliotron/Torsatron Plasmas, Oct 1998
(IAEA-CN-69/EX2/2)

NIFS-568 S. Okamura, K. Matsuoka, R. Akiyama, D S. Darrow, A. Ejiri, A. Fujisawa, M. Fujiwara, M. Goto, K. Ida H. Idei, H. Iguchi, N Inoue, M. Isobe, K. Itoh, S. Kado, K. Khlopenkov, T. Kondo, S. Kubo, A. Lazaros, S. Lee, G. Matsunaga, T. Minami, S Morita, S. Murakami, N. Nakajima, N. Nikai, S Nishimura, I. Nomura, S. Ohdachi, K. Ohkuni, M Osakabe, R. Pavlichenko, B. Peterson, R Sakamoto, H. Sanuki, M. Sasao, A. Shimizu, Y. Shirai, S. Sudo, S Takagi, C. Takahashi, S. Takayama, M Takechi, K Tanaka, K. Toi, K. Yamazaki, Y. Yoshimura and T. Watari,
Confinement Physics Study in a Small Low-Aspect-Ratio Helical Device CHS; Oct 1998
(IAEA-CN-69/OV4/5)

NIFS-569 M.M. Skonc, T. Sato, A. Maluckov, M.S Jovanovic,
Micro- and Macro-scale Self-organization in a Dissipative Plasma, Oct 1998

NIFS-570 T. Hayashi, N. Mizuguchi, T-H Watanabe, T. Sato and the Complexity Simulation Group,
Nonlinear Simulations of Internal Reconnection Event in Spherical Tokamak; Oct 1998
(IAEA-CN-69/TH3/3)

NIFS-571 A. Iiyoshi, A. Komori, A. Ejiri, M. Emoto, H. Funaba, M. Goto, K. Ida, H. Idei, S. Inagaki, S. Kado, O Kaneko, K. Kawahata, S. Kubo, R Kumazawa, S. Masuzaki, T. Minami, J. Miyazawa, T. Morisaki, S. Morita, S. Murakami, S. Muto, T. Muto, Y Nagayama, Y Nakamura, H. Nakanishi, K. Narihara, K. Nishimura, N. Noda, T. Kobuchi, S. Ohdachi, N Ohyabu, Y. Oka, M. Osakabe, T. Ozaki, B.J. Peterson, A. Sagara, S. Sakakibara, R. Sakamoto, H. Sasao, M. Sasao, K. Sato, M. Sato, T. Seki, T Shimozuma, M. Shoji, H. Suzuki, Y. Takeiri, K. Tanaka, K. Toi, T. Tokuzawa, K. Tsumori, I. Yamada, H Yamada, S. Yamaguchi, M. Yokoyama, K.Y.Watanabe, T Watari, R. Akiyama, H. Chikaraishi, K. Haba, S. Hamaguchi, S. Iima, S. Imagawa, N Inoue, K. Iwamoto, S. Kitagawa, Y. Kubota, J. Kodaira, R. Maekawa, T Mito, T Nagasaka, A Nishimura, Y Takita, C. Takahashi, K. Takahata, K. Yamauchi, H. Tamura, T. Tsuzuki, S. Yamada, N. Yanagi, H Yonezu, Y. Hamada, K Matsuoka, K Murai, K. Ohkubo, I. Ohtake, M Okamoto, S. Sato, T. Satow, S Sudo, S Tanahashi, K Yamazaki, M Fujiwara and O Motojima,
An Overview of the Large Helical Device Project; Oct 1998
(IAEA-CN-69/OV1/4)

NIFS-572 M. Fujiwara, H. Yamada, A. Ejiri, M. Emoto, H. Funaba, M. Goto, K. Ida, H Idei, S. Inagaki, S Kado, O. Kaneko, K. Kawahata, A. Komori, S. Kubo, R. Kumazawa, S. Masuzaki, T. Minami, J Miyazawa, T Morisaki, S Morita, S. Murakami, S. Muto, T. Muto, Y. Nagayama, Y. Nakamura, H. Nakanishi, K. Narihara, K. Nishimura, N Noda, T. Kobuchi, S. Ohdachi, N Ohyabu, Y. Oka, M. Osakabe, T. Ozaki, B. J. Peterson, A. Sagara, S. Sakakibara, R. Sakamoto, H. Sasao, M. Sasao, K. Sato, M. Sato, T Seki, T. Shimozuma, M. Shoji, H Sazuki, Y Takeiri, K. Tanaka, K Toi, T. Tokuzawa, K. Tsumori, I. Yamada, S Yamaguchi, M. Yokoyama, K.Y. Watanabe, T Watari, R. Akiyama, H. Chikaraishi, K. Haba, S. Hamaguchi, M Iima, S Imagawa, N Inoue, K. Iwamoto, S. Kitagawa, Y Kubota, J Kodaira, R Maekawa, T. Mito, T. Nagasaka, A. Nishimura, Y Takita, C Takahashi, K Takahata, K. Yamauchi, H. Tamura, T Tsuzuki, S. Yamada, N. Yanagi, H. Yonezu Y. Hamada, K. Matsuoka, K. Murai, K. Ohkubo, I. Ohtake, M. Okamoto, S. Sato, T Satow, S Sudo, S. Tanahashi, K. Yamazaki, O Motojima and A. Iiyoshi,
Plasma Confinement Studies in LHD; Oct. 1998
(IAEA-CN-69/EX2/3)

NIFS-573 O. Motojima, K. Akaishi, H. Chikaraishi, H. Funaba, S. Hamaguchi, S Imagawa, S. Inagaki, N. Inoue, A. Iwamoto, S. Kitagawa, A Komori, Y Kubota, R. Maekawa, S. Masuzaki, T. Mito, J Miyazawa, T Morisaki, T. Muroga, T Nagasaka, Y Nakmura, A. Nishimura, K. Nishimura, N. Noda, N Ohyabu, S Sagara, S Sakakibara, R Sakamoto, S Satoh, T. Satow, M. Shoji, H. Suzuki, K. Takahata, H. Tamura, K. Watanabe, H. Yamada, S. Yamada, S Yamaguchi, K. Yamazaki, N. Yanagi, T. Baba, H. Hayashi, M. Iima, T. Inoue, S Kato, T. Kato, T. Kondo, S. Moriuchi, H Ogawa, I. Ohtake, K. Ooba, H. Sekiguchi, N. Suzuki, S. Takami, Y. Taniguchi, T. Tsuzuki, N. Yamamoto, K. Yasui, H. Yonezu, M. Fujiwara and A Iiyoshi,
Progress Summary of LHD Engineering Design and Construction; Oct. 1998
(IAEA-CN-69/FT2/1)

NIFS-574 K Toi, M. Takechi, S. Takagi, G. Matsunaga, M Isobe, T. Kondo, M Sasao, D S Darrow, K Ohkuni, S. Ohdachi, R Akiyama A. Fujisawa, M Gotoh, H. Idei, K. Ida, H Iguchi, S. Kado, M Kojima, S Kubo, S Lee, K. Matsuoka, T Minami S. Morita, N Nikai, S. Nishimura, S. Okamura, M. Osakabe, A Shimizu, Y Shirai, C Takahashi, K Tanaka, T Watari and Y. Yoshimura,
Global MHD Modes Excited by Energetic Ions in Heliotron/Torsatron Plasmas; Oct. 1998
(IAEA-CN-69/EXP1/19)

NIFS-575 Y Hamada, A. Nishizawa, Y. Kawasumi, A. Fujisawa, M. Kojima, K Narihara, K Ida, A. Ejiri, S Ohdachi, K. Kawahata, K. Toi, K. Sato, T. Seki, H. Iguchi, K Adachi, S. Hidekuma, S.Hirokura, K. Iwasaki, T. Ido, R. Kumazawa, H. Kuramoto. T. Minami, I Nomura, M. Sasao, K.N. Sato, T Tsuzuki, I. Yamada and T Watari,
Potential Turbulence in Tokamak Plasmas; Oct. 1998
(IAEA-CN-69/EXP2/14)

NIFS-576 S. Murakami, U. Gasparino, H. Idei, S. Kubo, H. Maassberg, N. Marushchenko, N. Nakajima, M Romé and M. Okamoto,
5D Simulation Study of Suprathermal Electron Transport in Non-Axisymmetric Plasmas; Oct. 1998
(IAEA-CN-69/THP1/01)

NIFS-577 S. Fujiwara and T. Sato,
Molecular Dynamics Simulation of Structure Formation of Short Chain Molecules; Nov. 1998